European Journal of Radiology 102 (2018) 22–29

Contents lists available at ScienceDirect

European Journal of Radiology

journal homepage: www.elsevier.com/locate/ejrad

Research article

Brain white matter microstructural alterations in children of type I Gaucher disease characterized with diffusion tensor MR imaging

Huiying Kang[a,b,1], Miao Zhang[a,1], Minhui Ouyang[b], Ruolan Guo[c,d,e], Qinlin Yu[b,f,g], Qinmu Peng[b], Ningning Zhang[a], Yonghong Zhang[h], Yanlong Duan[h], Xiaolu Tang[a], Virendra Mishra[i], Fang Fang[f,g], Wei Li[c,d,e], Hao Huang[b,j], Yun Peng[a,*]

[a] Department of Radiology, Beijing Children's Hospital, Capital Medical University, Beijing, National Center for Children's Health, China
[b] Department of Radiology, Children's Hospital of Philadelphia, PA, United States
[c] Center for Medical Genetics, Beijing Pediatric Research Institute, Beijing Children's Hospital, Capital Medical University, National Center for Children's Health, China,
[d] MOE Key Laboratory of Major Diseases in Children, China
[e] Beijing Key Laboratory for Genetics of Birth Defects, China
[f] Peking University, School of Psychological and Cognitive Sciences, Beijing, China
[g] Peking University, Peking-Tsinghua Center for Life Sciences, Beijing, China
[h] Hematology Oncology Center Beijing Children's Hospital, Capital Medical University, National Center for Children's Health, Beijing, China
[i] Cleveland Clinic Lou Ruvo Center for Brain Health, Las Vegas, NV, United States
[j] Department of Radiology, Perelman School of Medicine, University of Pennsylvania, PA, United States

ARTICLE INFO

Key words:
Gaucher disease
Children
Diffusion tensor imaging
White matter

ABSTRACT

Objectives: To investigate white matter (WM) microstructural alterations in type I Gaucher disease (type I GD) pediatric patients and explore the correlation between the disease duration and WM changes.
Methods: Twenty-two GD patients and twenty-two sex- and age-matched typical development (TD) children were recruited. Changes in WM were investigated using diffusion tensor imaging (DTI) and applying atlas-based tract analysis. For all DTI measurements, independent-samples *t*-test was applied to report significant differences between type I GD and TD. Partial correlation was applied to determine whether the disease duration was correlated with DTI measurements.
Results: Bidirectional fractional anisotropy (FA) changes were found in the bilateral superior cerebellar peduncle, right posterior limb of the internal capsule, right posterior corona radiata, and right posterior thalamic radiation ($p < 0.05$). Higher mean diffusivity (MD)was found in the right superior corona radiata, middle cerebellar peduncle, right posterior thalamic radiation and right superior longitudinal fasciculus ($p < 0.05$) in type I GD. And higher radial diffusivity (RD) was also found in the left superior cerebellar peduncle ($p < 0.05$) in type I GD. The disease duration of type I GD patients is positively correlated with axial diffusivity and MD in multiple major WM tracts.
Conclusion: DTI findings supported the microstructural alterations of multiple WM tracts in type I GD patients.

1. Introduction

Gaucher disease (GD) is the most prevalent inherited lysosomal storage disorder resulting from the deficiency of the lysosomal enzyme glucocerebrosidase caused by the mutations in Beta-Glucocerebrosidase (GBA) gene. The overall frequency is approximately 1:40,000 to 1: 50,000 in the general population [1]. The accumulation of enzyme's major substrate, glucosylceramide, in multiple organ systems can lead

Abbreviations: WM, white matter; Type I GD, type I Gaucher disease; TD, typical development; DTI, diffusion tensor Imaging; FA, fractional anisotropy; MD, mean diffusivity; AD, Axial diffusivity; RD, radial diffusivity; GBA, beta-glucocerebrosidase; ERT, enzyme replacement therapy; TBSS, tract-based spatial statistics; IRB, institutional review board; FDR, false discovery rate; CFR, crossing-fiber region; SCP, superior cerebellar peduncle; PLIC-R, right posterior limb of internal capsule; PCR-R, right posterior corona radiata; PTR-R, right posterior thalamic radiation; SCR-R, right superior corona radiata; PCR-R, right posterior corona radiata; PTR-R, right posterior thalamic radiation; SCR-R, right superior corona radiata; MCP, middle cerebellar peduncle; PTR-R, right posterior thalamic radiation; SLF-R, right superior longitudinal fasciculus; ACR-L, left anterior corona radiata; ALIC-R, right anterior limb of the internal capsule; ACR-R, right anterior corona radiata; GCC, genu of corpus callosum

* Corresponding author at: Department of Radiology, Beijing Children's Hospital, Capital Medical University, National Center for Children's Health, No. 56 Nanlishi Road, West District, Beijing, 100045, China.
E-mail address: ppengyun@yahoo.com (Y. Peng).
[1] These two authors contributed equally to this work.

https://doi.org/10.1016/j.ejrad.2018.02.014
Received 27 August 2017; Received in revised form 7 January 2018; Accepted 11 February 2018

to hepatosplenomegaly, hypersplenism, destructive skeletal disease, bone marrow compromise, and nerve symptoms. Based on the presence or absence and rate of progression of neurological manifestations, the classical classification divides the disease into three subtypes: non-neuronopathic subtypes (i.e., type I), acute neuronopathic subtypes (i.e., type II), and chronic neuronopathic subtypes (i.e., type III), with more than 94% of patients with GD classified as the non-neuropathic subtype [2]. However, the traditionally deemed classification is challenged by recent findings. Previous clinical study reported that about 30% of patients with type I GD had at least one neurological symptom [3]. Moreover, an autopsy study observed astrogliosis in cerebral cortical layers 3 and 5, hippocampal CA2–4, and layer 4b in patients with types I, II, and III GD, who manifested neurodegeneration in these brain regions [4]. It has been suggested that GD's neuropathology process should be considered as a continuum phenotype, rather than a discrete predefined classification [3]. The early detection and dynamic monitoring of the changes in the central nervous system in childhood should be reinforced because neurological involvement may advance gradually. It can provide valuable insights to understand the pathology of brain changes in GD. It may provide more information on the potential neuropathological involvement of type I GD and give a clue to the prognosis.

Diffusion tensor imaging (DTI) is a noninvasive neuroimaging technique widely used in a variety of studies to quantify white matter (WM) microstructural properties and virtually reconstruct WM pathways in the living brain [5]. Atlas-based tract analysis surveys all major WM tracts for group comparisons of DTI-derived metrics [e.g. 6–8] and correlations [e.g. 8] with important variables such as age, clinical scores, disease duration. This analysis, integrated with the skeletonization process from tract-based spatial statistics (TBSS) that alleviate partial volume effects, yields observer-independent and hypothesis-free results. To date, brain imaging studies in patients with type I GD are limited. Typically, only a few patients were included in previous GD imaging studies. This may be due to the rarity of patients with GD. Scattered small, diffuse areas of brain WM changes were seen in the whole brain of patients with type I GD compared with normal volunteers in a DTI study [9]. Despite this preliminary finding, it remains unclear whether specific structural changes occur in the brain of p patients with type I GD.

This study hypothesized that the children with type I GD would show WM microstructural alterations before obvious clinical symptoms. The study used DTI and atlas-based tract analysis to examine WM structural abnormalities in patients with type I GD compared with healthy controls. A considerable amount of pediatric patients with type I GD (n = 22) and same amount of age-matched controls (n = 22) were included to test statistical significance and reliability of findings. The present study for patients with GD provides a proof-of-concept to identify possible early neuroimaging markers for the future clinical course.

2. Materials and methods

2.1. Participants

All participants were children recruited at Beijing Children's Hospital. About 22 children with type I GD (7 males and 15 females; mean age, 11.4 ± 3.3 years) and 22 children with TD (7 males and 15 females; mean age, 11.4 ± 3.5 years) participated in this study. The diagnoses of GD were established by measuring glucocerebrosidase activity in leukocytes or bone marrow and finding Gaucher cells. All patients, showing no obvious neurologically symptom, were diagnosed with type I GD by a hematologist and were under regular ERT. The exclusion criterion for children with GD was hemorrhage or other abnormality in the brain on routine MRI. The 22 children with TD at the time of MR imaging were referred for suspicion of precocious puberty (n = 5), intermittent headache (n = 9), and suspicion of short stature (n = 8). All these children had normal neurological examination outcome documented in medical record and identified as children with TD. The exclusion criteria for children with TD include known nervous system disease, or history of psychiatric, neurodevelopmental or systemic illness. Routine MRI imaging was normal for all GD patients and TD children. The Institutional Review Board (IRB) of the Beijing Children's Hospital approved the protocol, and written informed consent was obtained from parents or legal guardian of each patient.

2.2. Mutation analysis by direct sequencing

Genomic DNA was extracted from peripheral blood samples by standard methods. All coding regions and intron/exon boundaries of GBA gene were applied by the nested polymerase chain reaction (Nested-PCR). All the PCR primers were designed using Primer 5 software (Premier Biosoft International, Palo Alto, CA) (Supplementary Table 1). PCR products were purified by the DNA gel extraction kit (Qiagen, Valencia, CA) and sent for direct sequencing. Sequencing results were analyzed and alleles assigned with Mutation Surveyor version 5.0 (SoftGenetics) by comparing samples to reference sequences after alignment.

2.3. Data acquisition

MRI was performed using the Philips Achieva3T scanner (Philips Healthcare, Best, The Netherlands) with an eight-channel phased-array head coil. Foam padding was used to stabilize the patient's head position during the scanning. DTI data were acquired using a single-shot, echo-planar imaging sequence with the Sensitivity Encoding parallel imaging scheme (SENSE, reduction factor = 2). The imaging matrix size was 128 × 128 with a field of view of 256 × 256 mm^2. Axial slices of 2 mm thickness were acquired parallel to the anterior–posterior commissure (AC–PC) line. A total of 70 slices covered the entire brain without a slice gap. The repetition time and echo time were 7.96 s and 83 ms, respectively. Diffusion weighting was encoded along 30 independent directions, and the *b*-value was 1000 s/mm^2. One b0 image with 2 averages was acquired in the DTI data acquisition.

2.4. Atlas-based tract analysis

The DTI data were corrected for the effects of eddy currents and head motion by registering all diffusion weighted images (DWI) to a single b0 (nondiffusion sensitized) image using a 12-parameter (affine) linear image registration with automated image registration algorithm in DTIStudio. Then, the standard tensor fitting was conducted to generate the measurements such as fractional anisotropy (FA), mean diffusivity (MD), axial diffusivity (AD), and radial diffusivity (RD) with DTI Studio (https://www.mristudio.org/). Atlas-based tract analysis elaborated in the previous studies [6–8] was used for group comparisons. This approach integrated the digital WM atlas (JHU ICBM-DTI-81 atlas), and nonlinear registration, skeletonization and projection steps from TBSS of FMRIB Software Library (FSL) (http://fsl.fmrib.ox.ac.uk/fsl/fslwiki/TBSS). FA data of all subjects were aligned to a single-subject FA map ("EVE" template) used to generate JHU ICBM-DTI-81 atlas. Then, an FA skeleton mask was created by registering FA maps of all subjects to a mean FA map in JHU atlas space. In this way, the atlas labeling is overlaid to the mean skeleton in the ICBM-DTI-81 space such that each skeleton voxel could be categorized into one major tract. "Randomize" in FSL, adjusted for age, was used to analyze the differences between patients with GD and TD. A false discovery rate (FDR) correction at the cluster level threshold of $p < 0.05$ corrected for multiple comparisons. To avoid false-positive results, significant clusters containing ≥4 voxels were retained. RD, AD, and MD values were projected onto the skeleton mask obtained from mean FA image and compared between GD and TD groups using the aforementioned procedures. To ensure that the clusters were not caused by the crossing

fibers, planar anisotropy (CP) was calculated as follows: $2(\lambda_2 - \lambda_3)/(\lambda_1 + \lambda_2 + \lambda_3)$ of each voxel [10] All the voxels with CP > 0.2 were marked as crossing-fiber region (CFR) voxels [10,11]. The percentage of the CFR voxels in each cluster was calculated.

2.5. Statistical analyses

Statistical analyses were performed using SPSS (SPSS, IL, USA). Two-sample *t* tests were applied to determine whether a significant age discrepancy existed between patients with type I GD and TD, and a chi-squared test was applied to determine whether a significant discrepancy existed in sex distribution between the groups.

Partial correlation was conducted to investigate whether any correlation existed between disease duration and regional differences with all DTI-derived metric measurements corrected for age. To correct for multiple comparisons, a small-volume correction was made using FDR with an anatomically defined regional mask surrounding the cluster and consisting of skeleton voxels with 100 times the number of voxels of each cluster [12]. Only clusters with continuous voxels ≥5 and $p < 0.05$ (FDR corrected) were shown on the skeleton map.

3. Results

3.1. Demographics

Twenty-two patients with type I GD were compared with 22 children with TD were included in the present study. No significant differences in age or sex distribution were observed between patients with type I GD and TD. The average age of the patients and control subjects was 11.4 years (median 11.5, range 5.6–17.6) and 11.4 years (median 11.2, range 5.3–16.8), respectively ($P = 0.97$). In 15 of 22 patients, 68% were males, and in 15 of 22 control subjects, 68% were males ($P = 1$). The demographics and clinical features for type I GD and TD are presented in Table 1.

3.2. GBA gene mutations

As showed in Table 2 we successfully identified 16 different mutations from 22 GD patients. There are 12 pathogenic mutations reported in the Human Gene Mutation Database (S13L, R48Q, I93F, R120W, G202R, F213I, Y220C, L264I, G325R, V375L, M416V, L444P) and 4 new pathogenic mutations unreported before (L264V, R368H, p.L444W, p.D484_M489del). Three unreported missense mutations were predicted to be possibly damaging by the SIFT and Polyphen-2 web software.

L444P is the most frequent mutation accounting for 45.5% of the mutant alleles. The high prevalence of L444P consistent with the previous research in China population. [13] The other mutations with less frequency in our patients were L264I (6/44), V375L (4/44), M416V (2/44).

Table 1
Demographic and clinical characteristics of GD and TD subjects.

Group	Gaucher Disease Mean(SD)	Typical Development	p/χ2
Gender Male/Female	15/7	15/7	1
Age(years)	11.4(3.3)	11.4(3.5)	0.97
Disease duration (years)(only for GD)	8.4(2.2)	–	–
Time between treatment and MRI scan (years) (only for GD)	6.8(2.4)	–	–

Table 2
Genotypes of 22 GD patients.

Patient no.	Sex	age	Nucleotide change[*1]	Protein change
1	M	6.34	c.[475C > T(;) 907C > G[*2]]	p.R120W; p.L264V
2	M	5.59	c.[1240G > C(;) 1447_1448delinsTG[*2](;) 1450_1467del[*2]]	p.V375L; p.L444W; p.D484_M489del
3	M	7.41	c.[907C > A];[(907C > A)]	p.L264I; p.L264I
4	F	7.65	c.[1448T > C];[(1448T > C)]	p.L444P; p.L444P
5	M	8.76	c.[1240G > C];[?] [*3]	p.V375L;?
6	M	10.21	c.[754T > A(;) 1448T > C]	p.F213I; p.L444P
7	F	10.18	c.[394A > T(;) 1448T > C]	p.I93F; p.L444P
8	F	11.38	c.[1448T > C]; [(1448T > C)]	p.L444P; p.L444P
9	M	12.08	c.[776A > G(;) 907C > A]	p.Y220C; p.L264I
10	F	14.91	c.[1448T > C]; [(1448T > C)]	p.L444P; p.L444P
11	M	16.11	c.[907C > A(;) 1448T > C]	p.L264I; p.L444P
12	F	17.61	c.[1363A > G(;) 1448T > C]	p.M416V; p.L444P
13	M	13.84	c.[1448T > C]; [(1448T > C)]	p.L444P; p.L444P
14	M	15.84	c.[155C > T(;) 721G > A]	p.S13L; p.G202R
15	M	9.52	c.[1448T > C];[?][*3]	p.L444P;?
16	F	11.56	c.[1240G > C];[?] [*3]	p.V375L;?
17	M	13.43	c.[260G > A(;) 1448T > C]	p.R48Q; p.L444P
18	M	8.68	c.[1448T > C]; [(1448T > C)]	p.L444P;p.L444P
19	F	12.15	c.[907C > A];[(907C > A)]	p.L264I; p.L264I
20	M	13.94	c.[1090G > A (;) 1103G > A[*2](;) 1448T > C]	p.G325R; p.R368H; p.L444P
21	M	13.79	c.[1363A > G(;) 1448T > C]	p.M416V; p.L444P
22	M	10.61	c.[1240G > C(;) 1448T > C]	p.V375L; p.L444P

*1 The reference sequences used are NM_001005741.2 (*GBA*), while the sequences of exon1 are untranslated region. The description of DNA sequence variants follows the recommendations from the web of HGVS (Human Genome Variation Society).

*2 Mutations unreported in HGMD or Clinvar.

*3 One allele (chromosomes) of *GBA* gene contains a variant (e.g. c.1240G > C), while a variant for the other allele is expected but not yet identified.

3.3. Group difference in DTI-derived measurements

DTI analysis revealed that WM in patients with type I GD was widely affected. Figs. 1–3 and Table 3 show that decreased FA in GD (*p* corrected < 0.05) was found in the bilateral superior cerebellar peduncle (SCP), right posterior limb of internal capsule tract (PLIC-R), and right posterior corona radiata (PCR-R) compared with TD. Also, increased FA in GD (*p* corrected < 0.05) was also found in the right posterior thalamic radiation (PTR-R). Moreover, MD measures increased (*P* corrected < 0.05) in the right superior corona radiata (SCR-R), middle cerebellar peduncle (MCP), right posterior thalamic radiation (PTR-R), and right superior longitudinal fasciculus (SLF-R) in GD patient group. Higher RD also found in GD group (*p* corrected < 0.05) in the left SCP. No clusters with significant differences in AD were found between type I GD and TD. Based on the analysis, the overlap mean percentage of CFR voxels in the identified FA clusters is 31.8 ± 0.7%. The overlap mean percentage of CFR voxels in the identified RD clusters is 29.9 ± 0.8%. And the overlap mean percentage of CFR voxels in the identified MD clusters is44.5 ± 0.4%. All the identified clusters in FA, RD and MD presented less than 50% voxels labeled as CFR. The CFR map from a representative subject was shown in the Fig. S1 in the supplemental materials. Therefore, it was thought that all these differences were not due to the crossing fibers.

3.4. Disease duration and DTI metrics in GD

In the GD sample, the disease duration was positively correlated with the MD value in the SCR-R ($r = 0.64$, $P = 0.002$). The disease duration was also positively correlated with the AD value in the PLIC-R ($r = 0.84$, $P = 0.0025$), left anterior corona radiata (ACR-L) ($r = 0.64$, $P = 0.0025$), genu of corpus callosum (GCC) ($r = 0.69$, $P = 0.0039$),

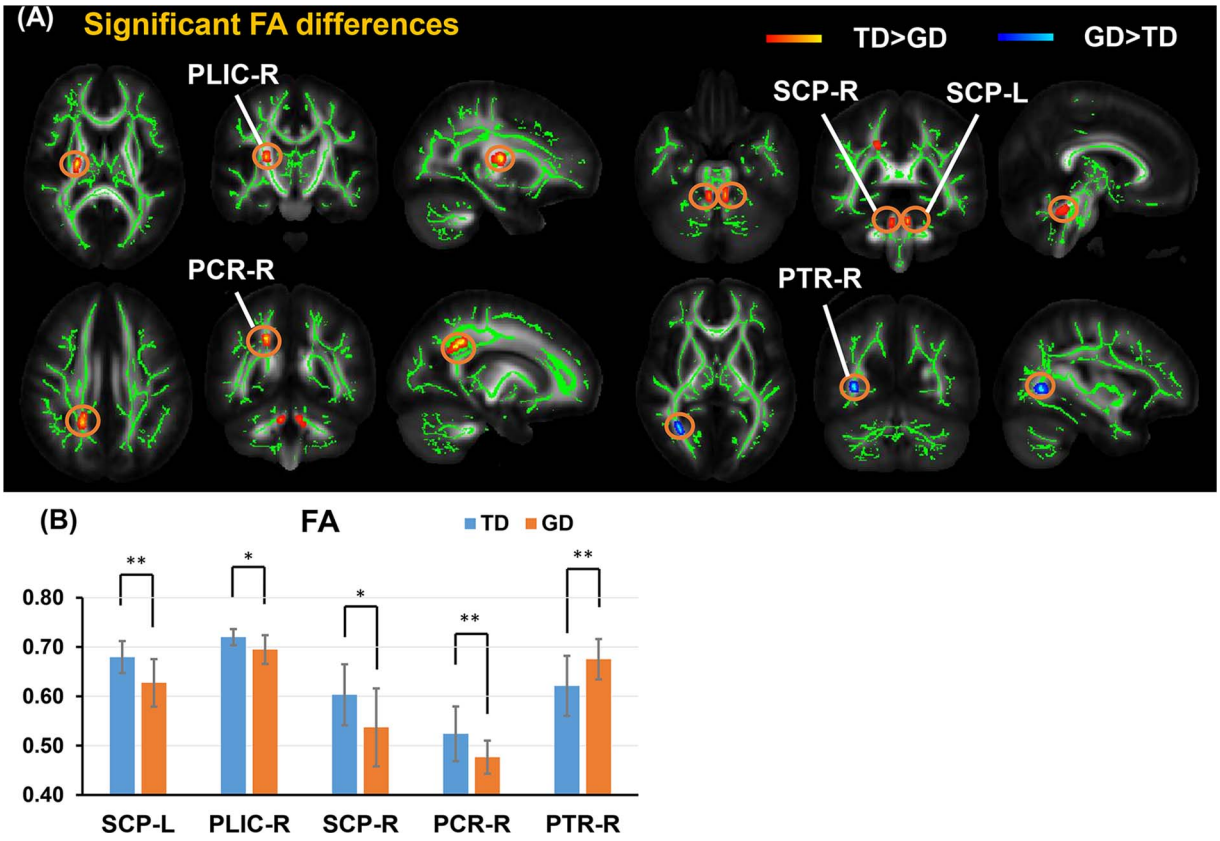

Fig. 1. (A) Significant bi-directional FA differences (red-yellow with TD > GD and blue-cyan for TD < GD) between GD and age-matched TD subjects. Significant clusters are superimposed on the white matter skeleton (green) obtained from averaged FA of all subjects. The background FA maps are averaged FA from ICBM-DTI-81 atlas. (B) Bar plot of mean FA values of GD patients and TD subjects. Tracts are identified with all FA maps mapped to the JHU ICBM-DTI-81 atlas space. L and R denote the left and right hemispheres. *FDR-corrected p &lt05. **FDR-corrected p&lt01. (For interpretation of the references to colour in this figure legend, the reader is referred to the web version of this article.)

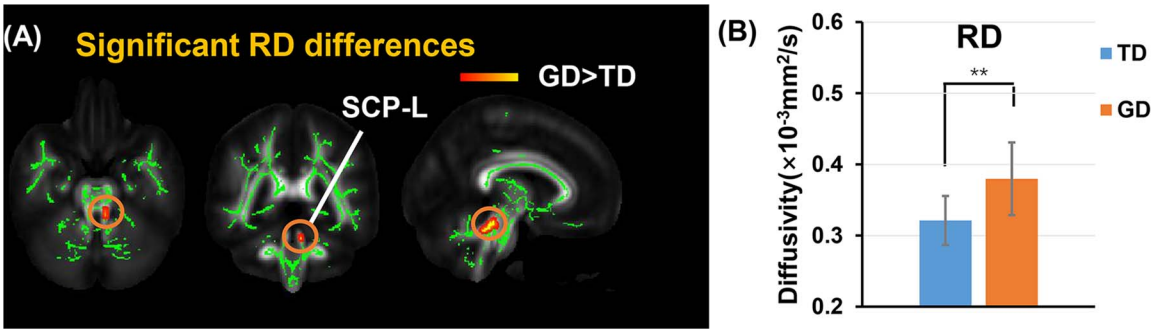

Fig. 2. (A) Exclusively higher RD (red-yellow) distributed in the WM were found in GD, compared to age-matched TD. Significant clusters are superimposed on the white matter skeleton (green) obtained from averaged FA of all subjects. The background FA maps are averaged FA from ICBM-DTI-81 atlas. (B) Bar plot of RD values of GD patients and TD subjects. Tract is identified with RD maps mapped to the JHU ICBM-DTI-81 atlas space. L and R denote the left and right hemispheres. *FDR-corrected $p < 0.05$. **FDR-corrected $p < 0.01$. (For interpretation of the references to colour in this figure legend, the reader is referred to the web version of this article.)

right anterior limb of the internal capsule (ALIC-R) ($r = 0.75$, $P = 0.0034$), and right anterior corona radiata (ACR-R) ($r = 0.71$, $P = 0.0025$). FA and RD were found to have no correlation with disease duration when controlled for age. (Table 4, Figs. 4 and 5).

4. Discussion

This was an original report focusing on the WM tract changes in patients with type I GD. The findings suggested that patients with type I GD manifested disruptions in several WM tracts related to the motor control, visuospatial function, and cognitive processes before obvious clinical manifestations of the nervous system. These DTI abnormalities provide valuable insight into the relationship between the microstructural alterations of WM pathways and clinical symptoms and possible neurophysiological mechanisms in patients with type I GD. The correlation of disease duration and DTI-derived metrics provide some focal monitoring items to the clinician for the follow-up of patients with type I GD.

FA is the most widely used DTI-derived metric inferring the WM microstructural property [14]. RD is thought to reflect decreased myelination [15]. AD could be associated with axonal degeneration [16]. The changes in MD values have also been described to be sensitive to WM microstructural disruption [17]. A combination of all these parameters might provide comprehensive information on the WM microstructural changes. In group comparison, higher MD and RD were seen in most areas. No significant group difference in AD was found. It indicated that for most areas WM involvement was more likely due to the demyelination in patients with type I GD. Bidirectional results in FA

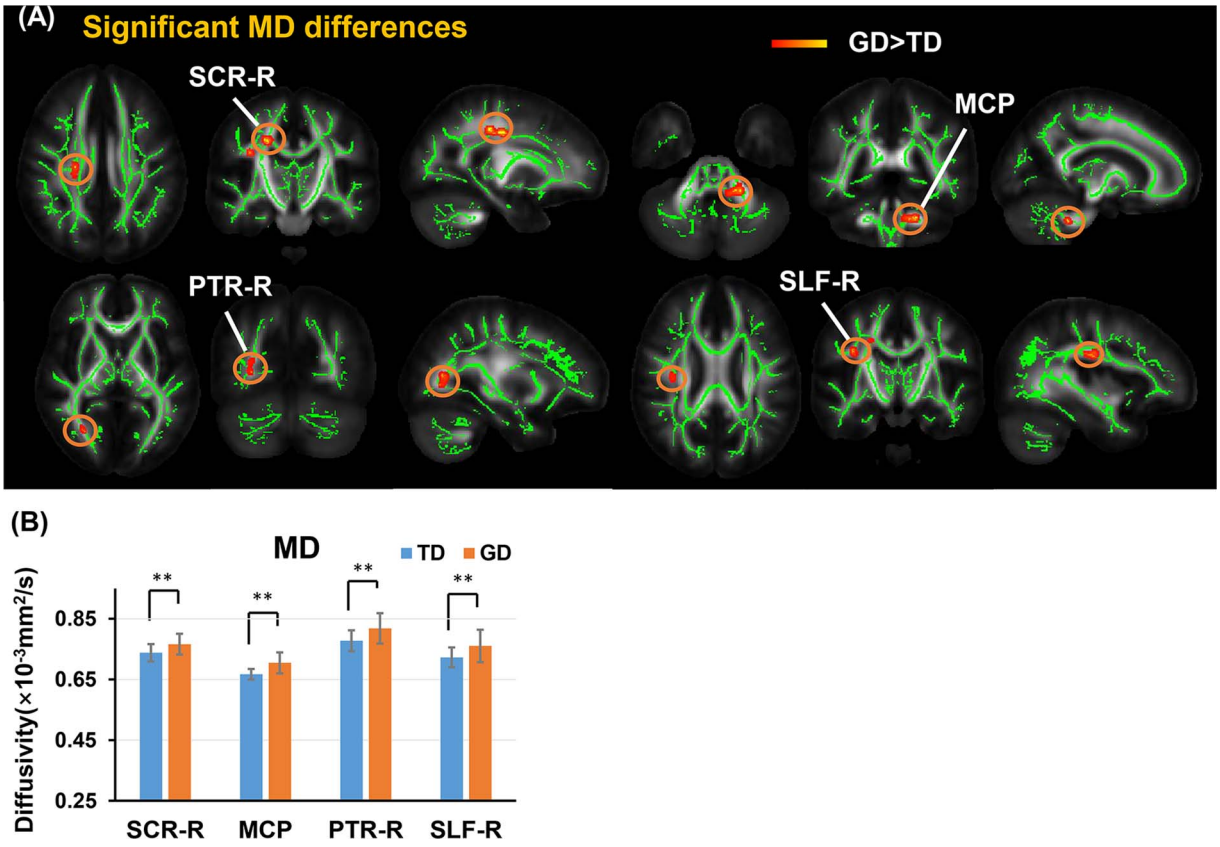

Fig. 3. (A) Exclusively higher MD (red-yellow) sparsely distributed in the WM were found in GD, compared to age-matched TD. Significant clusters are superimposed on the white matter skeleton (green) obtained from averaged FA of all subjects. The background FA maps are averaged FA from ICBM-DTI-81 atlas. (B) Bar plot of MD values of GD patients and TD subjects. Tracts are labeled with reference to the JHU ICBM-DTI-81 white-matter labels atlas. L and R denote the left and right hemispheres. *FDR-corrected $p < 0.05$. **FDR-corrected $p < 0.01$. (For interpretation of the references to colour in this figure legend, the reader is referred to the web version of this article.)

Table 3
FA, RD and MD values (mean ± standard deviation), number of skeleton voxels, t, and P values of the identified largest cluster in each affected WM tract from group comparison of FA RD and MD at skeleton voxels between GD and TD. L and R indicate left and right, respectively. Please see Fig. 1 legend for white matter tract abbreviations.

white matter tract	FA of TD (n = 22)	FA of GD (n = 22)	number of skeleton voxels	t	P
TD > GD					
SCP-L	0.68 ± 0.03	0.63 ± 0.05	9	4.20	0.0026
PLIC-R	0.72 ± 0.02	0.69 ± 0.03	7	3.52	0.0102
SCP-R	0.60 ± 0.06	0.54 ± 0.08	6	3.10	0.0114
PCR-R	0.52 ± 0.06	0.48 ± 0.03	5	3.41	0.0017
GD > TD					
PTR-R	0.62 ± 0.06	0.68 ± 0.04	6	3.46	0.0014

white matter tract	RD ($\times 10^{-3}$ mm^2/s) of TD(n = 22)	RD ($\times 10^{-3}$ mm^2/s) of GD(n = 22)	Number of skeleton voxels	t	P
GD > TD					
SCP-L	0.32 ± 0.03	0.38 ± 0.05	5	4.47	0.0031

white matter tract	MD ($\times 10^{-3}$ mm^2/s) of TD(n = 22)	MD ($\times 10^{-3}$ mm^2/s) of GD(n = 22)	of Voxels	t	P
GD > TD					
SCR-R	0.74 ± 0.03	0.77 ± 0.03	8	2.96	0.0118
MCP	0.67 ± 0.02	0.70 ± 0.03	6	4.52	0.0040
PTR-R	0.77 ± 0.03	0.82 ± 0.05	5	3.15	0.0032
SLF-R	0.72 ± 0.03	0.76 ± 0.05	5	2.83	0.0078

were also found. For most area, patients with type I GD showed lower FA. However, in the PTR-R, a higher FA was associated with higher MD. These changes might suggest different WM changes in these areas. In fact, although FA is considered as a direct marker of WM integrity, it may also be related to other factors including axonal count and density, degree of myelination, and fiber organization [18]. Combined with the increase in MD, it may reflect the selective neurodegeneration and lower neural branching.

Decreased FA in the bilateral SCP, increased RD in the SCP-L, and increased MD in the MCP were similar to the previous findings, including patients with both types I and III GD [9]. It is indicated that patients with types I and III GD may share similar WM involvement. The SCP and MCP are the major output and input pathways of the cerebellum and complete a circuit between the cerebral and cerebellar cortices. Their main function is related to coordinating the motor output of the cerebral cortex [19]. And in previous study about patients with diffuse periventricular leukomalacia and born preterm, it has been shown that the decreased FA in SCP and MCP is related to the pathophysiology of motor disability [20]. Bone marrow infiltration is one of the most common symptoms of both types I and III GD and leads to osteopenia, osteonecrosis, osteosclerosis, bone crises, chronic bone pain, pathological fracture, lytic lesions, and skeletal deformities which may be related to motor disability. Based on the previous MRI or X-ray exam patients with type I GD in this study suffered from varying degrees of skeletal infiltration. And some of them had complained about chronic pain. Furthermore some of them suffered from fracture and even underwent artificial femoral head replacement and had different degrees of unsteady gait and impaired fine and gross motor skills. Therefore, the complication of skeletal infiltration may be associated with the decrease of FA changes of cerebellar peduncle in patients with

Table 4
White matter regions where a significant partial correlation between MD or AD values and the disease duration was found. Number of skeleton voxels, r, and P values of the identified cluster in each affected WM tract at skeleton voxels in GD. L and R indicate left and right, respectively. Please see Fig. 1 legend for white matter tract abbreviations.

white matter tract	number of skeleton voxels	p	r
MD			
SCR-R	5	0.0245	0.64
white matter tract	number of skeleton voxels	p	r
AD			
PLIC-R	18	0.0025	0.84
ACR-L	7	0.0025	0.64
GCC	7	0.0039	0.69
ALIC-R	6	0.0034	0.75
ACR-R	5	0.0025	0.71

type I GD.

The alterations in FA and MD are also found in the PLIC-R, PCR-R, and SCR-R, which contain ascending fibers from the thalamus to the cerebral cortex and descending fibers from the frontoparietal cortex to subcortical nuclei and spinal cord. They are important WM modes that participate in the transfer of perceptual and motor functions and other higher cognitive functions [21]. Also, clusters with a significant difference in MD in SLF-R are found. SLF is a major fiber tract connecting the parietal, occipital, and temporal lobes with ipsilateral frontal cortices of each cerebral hemisphere [22]. It is necessary for core processes such as attention, memory, emotions, and language [23]. These changes may relate to poorer ability to focus attention and a slower retrieval of information held in memory found in patients with GD I [24].

Interestingly increased FA and MD were found in the PTR-R, which connects the pulvinar complex and lateral geniculate nucleus and the posterior parietal and occipital lobes of the cerebral cortex. It includes the optic radiation and is related to visuospatial function. The saccade

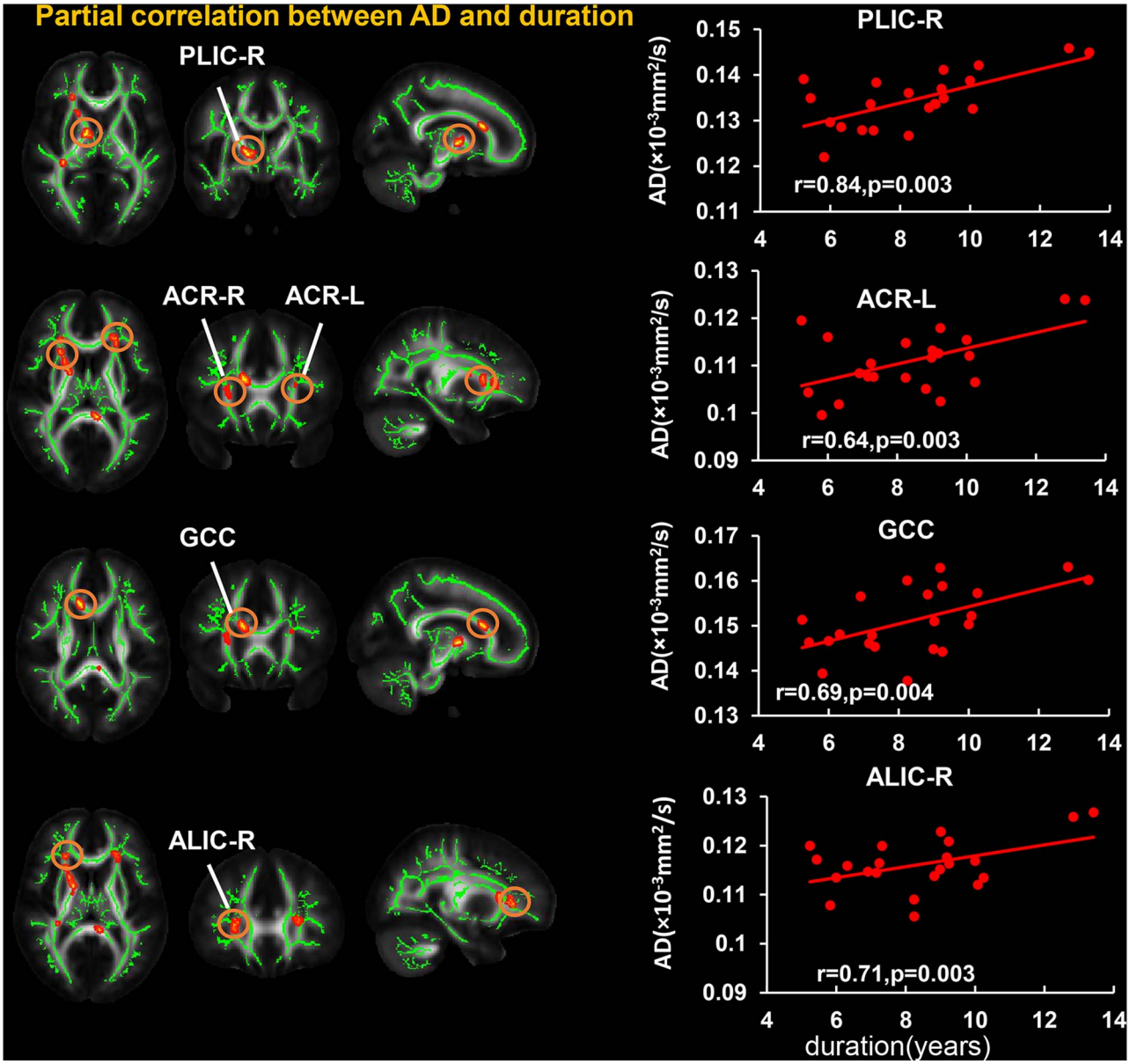

Fig. 4. Significant correlations between the disease duration and the AD in GD after controlling for age. The location and distributions of significant clusters are shown on the left panels. Scatter plots of AD from the cluster of GD are shown on the right panels. Each circle in the scatter plot represents AD measurement from one child with GD, respectively. The lines were linearly fitted from these measurements. R values are correlation coefficients of AD measurements and disease duration after controlling for age.

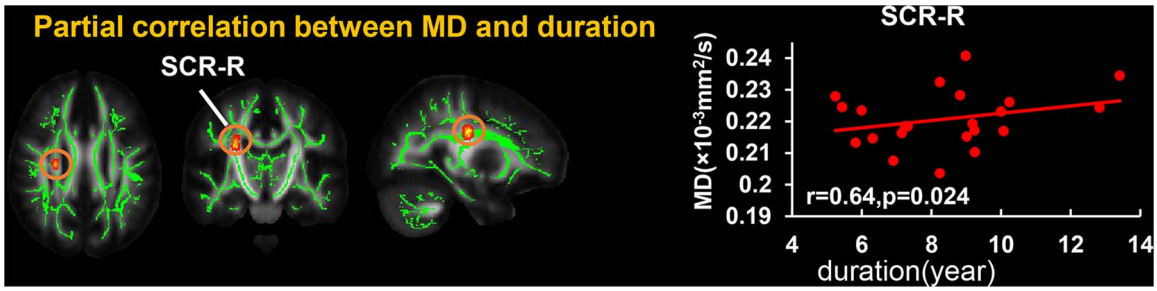

Fig. 5. Significant positive correlations between the disease duration and the MD in GD after controlling for age. The location and distributions of significant clusters are shown on the left panels. Scatter plots of MD from the cluster of GD are shown on the right panels. Each circle in the scatter plot represents MD measurement from one child with GD, respectively. The lines were linearly fitted from these measurements. R values are correlation coefficients of MD measurements and disease duration after controlling for age.

initiation failure (ocular motor apraxia and supranuclear gaze palsy) is often the earliest neurological sign in patients with type III GD [25], and it can be difficult to detect it clinically. These previous results together with the present findings indicate that patients with type I GD may have the microstructural changes in the visual pathway before obvious clinical symptoms. They provide a clue for further follow-up.

A positive correlation exists between MD, AD, and disease duration in multiple WM tracts including the commissural fibers and projection fibers. It indicates that AD may be more sensitive and suitable for monitoring the longitudinal changes in the disease. AD is defined as the longitudinal diffusion along axons, which is related to the status of axons or bundle coherence. [12,26]. Research shows that the reduced axonal density or caliber can lead to the increased AD because of the increasing axonal space, allowing axons to be straighter [27]. The involved projection tracts including PLIC-R, bilateral ACR, and ALIC-R, which are also involved in the group comparison, are related to perceptual motor functions and other higher cognitive functions [19]. The atypical microstructural changes in GCC, which is the large commissural tract indicating reduced interhemispheric connectivity via the corpus callosum, hence reduce interhemispheric inhibition or less long-range interaction control of the motor, perceptual, and cognitive functions [28,29]. It may indicate that more attention should be paid to the evaluation of the higher cognitive functions in the future follow-up of patients with GD.

Among all these microstructural changes, an interesting rightward asymmetry has been observed in multiple white matter tracts. Since there are limited imaging studies about GD patients, no similar findings were reported. However, previous study has shown the rightward FA asymmetry in normal population in the ALIC, PLIC, PTR, corona radiata, and SLF [30], which are similar tracts in our results. The rightward asymmetry of the DTI findings in the present study may be related to the asymmetry observed in the normal population.

Following limitations should be considered for this study. First, the patients' ages ranged from 7 to 18 years, which is a period of rapid physical development. Although the age was taken as a covariate, it was difficult to completely exclude the influence of growth. Next, all patients underwent ERT but the length of treatment differed across patients. Despite no evidence that the ERT can pass the blood–brain barrier, the secondary changes caused by the non-neurological symptoms and the correlation with disease duration may be affected by treatment. Furthermore, it will enhance our findings if the clinical scores (e.g. the motor ability and cognitive findings) were added to this study. Unfortunately, we didn't hypothesize that these clinical symptoms were possibly related to the white matter structural changes in type I GD patients at the beginning of this study. And the relevant clinical datasets were not included in this study Future studies should include more neurological and cognitive evaluation to elucidate the correlation between symptoms and structural changes.

In conclusion, this study identified microstructural alterations in multiple WM tracts in patients with type I GD before obvious symptoms. The findings suggested that the physician should reinforce the monitoring of early neurological and cognitive symptoms in patients with type I GD during the follow-up. DTI analysis could be a potential imaging marker to monitor changes in the brain of patients with type I GD.

Conflict of interest

None.

Acknowledgements

This study is sponsored by NIHR01MH092535, U54HD086984 and NSFC31271161 and 81671651.

Appendix A. Supplementary data

Supplementary data associated with this article can be found, in the online version, at https://doi.org/10.1016/j.ejrad.2018.02.014.

References

[1] Phenotype diagnosis, and treatment of Gaucher's disease, Lancet 372 (9645) (2008) 1263–1271.
[2] P. Kaplan, H.C. Andersson, K.A. Kacena, J.D. Yee, The clinical and demographic characteristics of nonneuropathic Gaucher disease in 887 children at diagnosis, Arch. Pediatr. Adolesc. Med. 160 (2006) 603–608.
[3] J.L. Capablo, A.S. de Cabezón, J. Fraile, P. Alfonso, M. Pocovi, P. Giraldo, Spanish Group on Gaucher Disease, Neurological evaluation of patients with Gaucher disease diagnosed as type 1, J. Neurol. Neurosurg. Psychiatry 79 (2) (2008) 219–222.
[4] Kondi Wong, E. Sidransky, A. Verma, et al., Neuropathology provides clues to the pathophysiology of Gaucher disease, Mol. Genet. Metab. 82 (3) (2004) 192–207.
[5] Denis Le Bihan, Looking into the functional architecture of the brain with diffusion MRI, Nat. Rev. Neurosci. 4 (6) (2003) 469–480.
[6] H. Huang, X. Fan, M. Weiner, et al., Distinctive disruption patterns of white matter tracts in Alzheimer's disease with full diffusion tensor characterization, Neurobiol. Aging 33 (9) (2012) 2029–2045.
[7] H. Huang, T. Gundapuneedi, U. Rao, White matter disruptions in adolescents exposed to childhood maltreatment and vulnerability to psychopathology, Neuropsychopharmacology 37 (12) (2012) 2693–2701.
[8] M. Ouyang, H. Cheng, V. Mishra, et al., Atypical age-dependent effects of autism on white matter microstructure in children of 2–7 years, Hum. Brain Mapp. 37 (2) (2016) 819–832.
[9] E.H. Davies, K.K. Seunarine, T. Banks, C.A. Clark, A. Vellodi, Brain white matter abnormalities in paediatric Gaucher Type I and Type III using diffusion tensor imaging, J. Inherit. Metab. Dis. 34 (2) (2011) 549–553.
[10] S.O. Peled Friman, F. Jolesz, C.F. Westin, Geometrically constrained two-tensor model for crossing tracts in DWI, Magn. Reson. Imaging 24 (9) (2006) 1263–1270.
[11] Virendra Mishra, X. Guo, M.R. Delgado, H. Huang, Toward tract-specific fractional anisotropy (TSFA) at crossing-fiber regions with clinical diffusion MRI, Magn. Reson. Med. 74 (6) (2015) 1768–1779.
[12] Amelia Versace, J.R. Almeida, S. Hassel, et al., Elevated left and reduced right orbitomedial prefrontal fractional anisotropy in adults with bipolar disorder revealed by tract-based spatial statistics, Arch. Gen. Psychiatry 65 (9) (2008) 1041–1052.
[13] Y. Feng, Y. Huang, C. Tang, et al., Clinical and molecular characteristics of patients with Gaucher disease in Southern China, Blood Cell Mol. Dis. 68 (2018) 30–34.
[14] Christian Beaulieu, The basis of anisotropic water diffusion in the nervous system–a technical review, NMR Biomed. 15 (7–8) (2002) 435–455.
[15] Sheng-Kwei Song, S.W. Sun, M.J. Ramsbottom, C. Chang, J. Russell, A.H. Cross, Dysmyelination revealed through MRI as increased radial (but unchanged axial) diffusion of water, Neuroimage 17 (3) (2002) 1429–1436.

[16] Shu-Wei Sun, H.F. Liang, K. Trinkaus, A.H. Cross, R.C. Armstrong, S.K. Song, Noninvasive detection of cuprizone induced axonal damage and demyelination in the mouse corpus callosum, Magn. Reson. Med. 55 (2) (2006) 302–308.
[17] C. Pierpaoli, A. Barnett, S. Pajevic, et al., Water diffusion changes in Wallerian degeneration and their dependence on white matter architecture, Neuroimage 13 (6) (2001) 1174–1185.
[18] Gavin P. Winston, The physical and biological basis of quantitative parameters derived from diffusion MRI, Quant. Imaging Med. Surg. 2 (4) (2012) 254–265.
[19] Cristina Granziera, J.D. Schmahmann, N. Hadjikhani, et al., Diffusion spectrum imaging shows the structural basis of functional cerebellar circuits in the human cerebellum in vivo, PLoS One 4 (4) (2009) e5101.
[20] S. Wang, G.G. Fan, K. Xu, et al., Altered microstructural connectivity of the superior and middle cerebellar peduncles are related to motor dysfunction in children with diffuse periventricular leucomalacia born preterm: a DTI tractography study, Eur. J. Radiol. 83 (6) (2014) 997–1004.
[21] Jeremy D. Schmahmann, N. Pandya Deepak, Disconnection syndromes of basal ganglia, thalamus, and cerebrocerebellar systems, Cortex 44 (8) (2008) 1037–1066.
[22] Jeremy D Schmahmann, E.E. Smith, F.S. Eichler, C.M. Filley, Cerebral white matter, Ann. N. Y. Acad. Sci. 1142 (1) (2008) 266–309.
[23] A. Kamali, A.E. Flanders, J. Brody, et al., Tracing superior longitudinal fasciculus connectivity in the human brain using high resolution diffusion tensor tractography, Brain Struct. Funct. 219 (1) (2014) 269–281.
[24] M. Biegstraaten, K.A. Wesnes, C. Luzy, et al., The cognitive profile of type 1 Gaucher disease patients, J. Inherit. Metab. Dis. 35 (6) (2012) 1093–1099.
[25] C.M. Harris, D.S. Taylor, A. Vellodi, Ocular motor abnormalities in Gaucher disease, Neuropediatrics 30 (6) (1999) 289–293.
[26] Andrew L. Alexander, J.E. Lee, M. Lazar, A.S. Field, Diffusion tensor imaging of the brain, Neurotherapeutics 4 (3) (2007) 316–329.
[27] M. Takahashi, J. Ono, K. Harada, M. Maeda, D.B. Hackney, Diffusional anisotropy in cranial nerves with maturation: quantitative evaluation with diffusion MR imaging in rats, Radiology 216 (3) (2000) 881–885.
[28] Mitchell Glickstein, Giovanni Berlucchi, Classical disconnection studies of the corpus callosum, Cortex 44 (8) (2008) 914–927.
[29] Karl W. Doron, Michael S. Gazzaniga, Neuroimaging techniques offer new perspectives on callosal transfer and interhemispheric communication, Cortex 44 (8) (2008) 1023–1029.
[30] H. Takao, N. Hayashi, K. Ohtomo, White matter microstructure asymmetry: effects of volume asymmetry on fractional anisotropy asymmetry, Neuroscience 231 (4) (2013) 1–12.